Reviews

Mercury and cadmium pnictidehalides: the inverted Zintl phases

A. V. Shevelkov and M. M. Shatruk*

Department of Chemistry, M. V. Lomonosov Moscow State University,
Leninskie Gory, 119899 Moscow, Russian Federation.
Fax: +7 (095) 939 4778. E-mail: shev@inorg.chem.msu.ru

The structures of the mercury and cadmium pnictidehalides $M_aZ_bX_c$ (M = Cd, Hg; Z = P, As, Sb; X = Cl, Br, I) are discussed on the basis of the Zintl—Klemm concept. Primary attention is paid to the relationship between the crystal and electronic structures of the compounds in question.

Key words: Zintl phases, pnictidehalides, crystal structure, solid-state chemistry, cadmium, mercury, pnicogen.

Introduction

The term "Zintl phases" entered the chemists´ vocabulary more than 50 years ago to reflect the merits of Edward Zintl, who had discovered and studied a new class of compounds intermediate between typical salts and intermetallics. The term "Zintl phases" has not received so far an exhaustive definition. Any attempt to classify Zintl phases turns on the impossibility of specifying clear borders between different classes of compounds.

Traditional Zintl phases are binary and ternary compounds, in whose crystal structures the cationic sublattices are made up of alkali and alkaline earth element atoms, while the anionic sublattices consist of Group 13—15 nontransition elements. In binary compounds consisting of electropositive cations A and post-transition elements B, the cation A transfers its electrons to element B, which thus achives a closed electron shell. The electron octet of element B appears due to the formation of two-electron covalent B—B bonds and localization of lone electron pairs.

A significant consequence of the fulfillment of the octet rule is the appearance of properties typical of most of Zintl phases. The fact that element B reaches a closed-shell electronic configuration implies that all the bonding and nonbonding (lone electron pairs) states in the covalent anionic sublattice are occupied, while all the antibonding states are vacant. Hence, the Zintl phases are dielectrics, even when element B is a metal, and exhibit diamagnetic properties. Owing to the fact that the difference between the electronegativities of elements A and B is relatively small, the band gap in the Zintl phases does not exceed 2.5 eV, unlike that in typical salts. Finally, since the number of electrons provided by element A strictly correlates with the number of B—B bonds and lone pairs of element B, the Zintl phases possess a very narrow homogeneity region.

The range of compounds that can be referred to as "Zintl phases" has now markedly extended.[1] First, the properties of some compounds described formally by the Zintl scheme differ from those predicted. These are so-called "metallic Zintl phases" formed by Group 13 and 14 elements and alkali metals.[2] When the octet rule

Published in Russian in *Izvestiya Akademii Nauk. Seriya Khimicheskaya,* No. 3, pp. 321—336, March, 2001.

1066-5285/01/5003-337 $25.00

formally holds, the change in the interaction energy on going from a local level to an extended system may result in the vanishing of the band gap giving rise to the metallic type of conductivity. Second, there exists a vast group of compounds formed by electropositive elements A and Group 13—15 elements that exhibit properties characteristic of Zintl phases but, nevertheless, have an electronic structure not conforming to the octet rule. As an example, note metal-rich lithium silicides and germanides,[3] whose electronic structures and properties are due to the occupation of the "cage" orbitals of Li clusters, as well as alkali and alkaline earth metal aluminides,[4] which are typically characterized by relatively high coordination numbers of aluminum (5 and 6). In addition, compounds containing transition metals,[5,6] in which the octet rule cannot be fulfilled but so-called completed electron configurations can be formed are classified as nontraditional Zintl phases.

A specific case of nontraditional Zintl phases is represented by compounds that we will call "inverted" Zintl phases. In these compounds, the cationic sublattice consists of post-transition elements having an electron octet and transfering excess electrons to electronegative elements, usually halogens. As examples, one can cite BiTeCl [7] and $(Ge_{43.33}I_{2.67})I_8$,[8] isotypical to the traditional Zintl phases KSnAs [9,10] and $K_8Sn_{44}\square_2$,[11] respectively.

Among the inverted Zintl phases, the family of cadmium and mercury pnictidehalides presents special interest because this family is vast (the number of the ternary phases alone is over 40), and the compounds belonging to it possess diverse crystal and electronic structures and exhibit different properties. Despite the diversity of crystal structures, virtually any cadmium and mercury pnictidehalide is constructed according to a common pattern: Group 12 and 15 elements form a three-dimensional positively charged framework due to cadmium (or mercury)—pnicogen and pnicogen—pnicogen covalent bonds, whereas halogen atoms serve as the counterions. The electronic configurations of elements are different. The pnicogen atoms form an electron octet, whereas the Cd and Hg atoms have a completed d^{10} configuration.

In this review, we demonstrate the diversity of the crystal structures of cadmium and mercury pnictidehalides, analyze the relationship between their crystal and electronic structures, show the possibility of using the Zintl approach for interpreting and predicting the properties of these phases, and outline the limitations of this approach.

Zintl phases: characteristic features of the electronic structure

Zintl phases are characterized by a strict correspondence between the crystal and electronic structures. The anionic sublattice in the crystal structure of NaTl is similar[12] to the structure of diamond (Fig. 1). Each Tl atom forms four homonuclear bonds with a tetrahedral

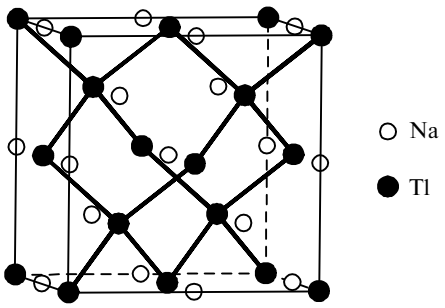

Fig. 1. Crystal structure of NaTl; the diamond-like network of thallium atoms is shown.

arrangement of neighbors. Since the Tl—Tl bond is two-electron, to form four bonds, the Tl atom must acquire one more electron, which is provided by the Na atom. Thus, the Tl atom forms an electron octet (four electron pairs in the four homonuclear bonds), its electron configuration representing that of carbon in diamond. In accordance with the classical Klemm concept, the Tl^- ion is a pseudo-element because it exhibits structural characteristics of an isoelectronic element.

The Zintl—Klemm approach is also applicable in those cases where atoms of two elements form simultaneously an anionic sublattice. In the crystal structure of KSnAs,[9] the Sn and As atoms form corrugated layers and the K atoms are located between them (Fig. 2). Each Sn and As atom forms three bonds arranged pyramidally and has a lone pair. The resulting electronic configuration, ns^2np^3, indicates As^0 and Sn^- (pseudo-element isostructural to arsenic). In view of the lower electronegativity of tin, the description of the distribution of formal oxidation states as $K^+Sn^-As^0$ appears ungrounded. An alternative description of the electronic

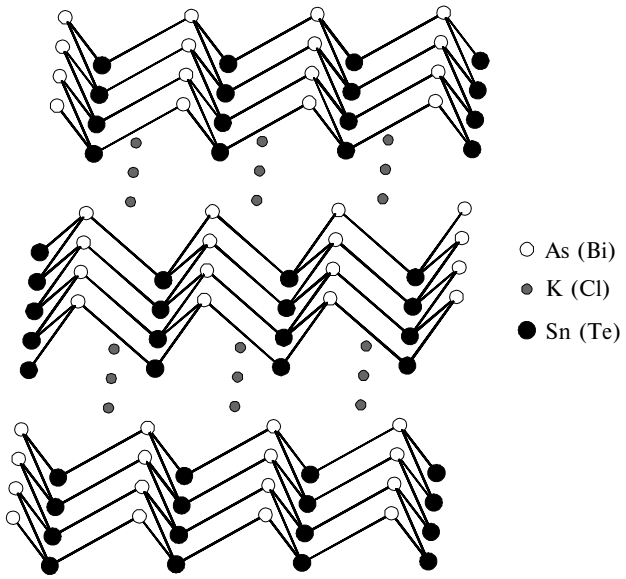

Fig. 2. Fragment of the crystal structures of KSnAs and BiTeCl; the corrugated layers of Sn and As (Te and Bi) atoms separated by K (Cl) atoms are shown.

structure is based on the ionic approach to the Sn—As bond. With this extreme polarization, the electronic configurations are $4s^24p^6$ for arsenic and $5s^25p^0$ for tin. However, the slight difference between the electronegativities of tin and arsenic rules out the possibility of the ionic scheme $K^+Sn^{2+}As^{3-}$. The real distribution of oxidation states is intermediate between these two extreme schemes; the description $K^+[SnAs]^-$ is the most plausible. The isostructural compound KSnSb **10** can also be represented as $K^+[SnSb]^-$. The calculations of band structure**13** and the Mössbauer spectroscopy data**14** for KSnSb do not allow assignment of unambiguous oxidation numbers to Sn or Sb.

By comparing the crystal structures of KSnAs and BiTeCl,**7** one can easily see that these compounds are "anti-isotypical." In the latter compound (see Fig. 2), the Bi and Te atoms form corrugated layers separated by Cl atoms. The electronic structures of two compounds are also symmetric. In the BiTeCl structure, the Bi and Te atoms form two-center two-electron bonds and lend excess electrons to the Cl atoms. The electronegativity of tellurium is only slightly higher than that of bismuth; therefore, the extreme formulas, $Bi^0Te^+Cl^-$ (based on the Klemm pseudo-atoms) and $Bi^{3+}Te^{2-}Cl^-$ (based on the purely ionic model), are inapplicable, while the formula $[BiTe]^+Cl^-$ is more appropriate. Comparison of the crystal and electronic structures of the two compounds shows that the formal charges in BiTeCl have been inverted, crystal structure principles being retained; therefore, the use of the term the "inverted" Zintl phase for BiTeCl is quite justified.

The description of the Zintl phases containing transition metals is faced with additional complications. The stability of some d-configurations should be taken into account.**15** This refers to certain low-spin states, namely, d^8 in a square environment and d^6 in an octahedral environment. We will consider the family of compounds with the general formula MP_4. As an example, Fig. 3 shows the structure of FeP_4 in which the metal atoms are octahedrally surrounded by P atoms. MgP_4 is a traditional Zintl phase, in which magnesium acts as the cation.**16** In this case, the conventional Zintl scheme of electron counting can be used. The electropositive metal (magnesium) transfers two electrons giving rise to the $_\infty{}^2(P_2{}^{4-})$ polyanion, whose electronic structure is described adequately from the standpoint of the octet rule. In FeP_4, RuP_4, and OsP_4 **17,18** having a similar structure, the d-metal in the oxidation state +2 possesses a "completed" $t_{2g}{}^6$ configuration. Finally, in CdP_4,**19** the post-transition metal (cadmium) in the oxidation state +2 acquires a different variant of a stable electronic configuration, namely, d^{10}.

The classical Zintl scheme, according to which element A only gives its electrons for atoms of the anion to form an electron octet, is inapplicable for the discussion of chemical bonding in compounds formed by the A cations with a stable d-configuration. An alternative to this scheme is to consider the covalent metal—ligand

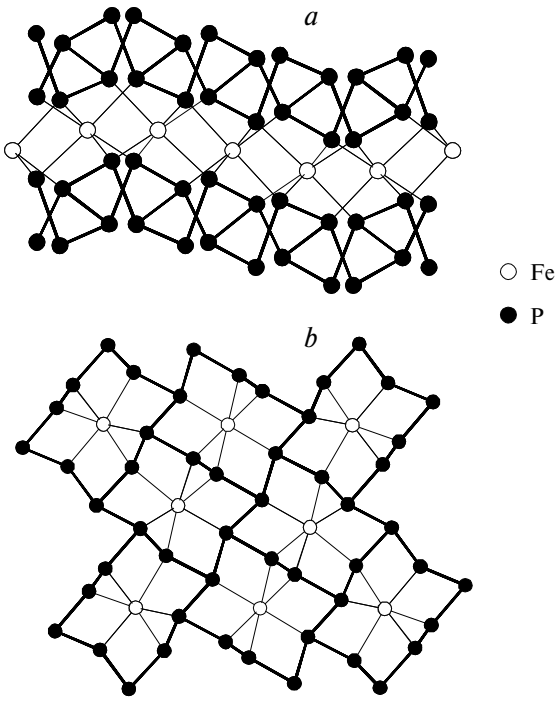

Fig. 3. View of the crystal structure of FeP_4 along (*a*) and across (*b*) the direction of extension of the $_\infty{}^2(P_4{}^{2-})$ layers; the bold lines show the P—P bonds.

interaction in terms of the approach used in the ligand-field theory. The scheme of splitting of d-metal orbitals in an octahedral ligand environment, shown in Fig. 4 as an example, demonstrates that in the d^6-configuration, all the bonding and nonbonding MO are occupied, while all the antibonding orbitals remain vacant; this is what is required for the Zintl phases. In this respect, the d^6 ($t_{2g}{}^6$)-configuration of an octahedral cation can be referred to as a completed configuration. Hence, when the octet rule is fulfilled for the main-group element, it is easy to predict the properties typical of the Zintl phases, namely, dielectric and diamagnetic properties.

Unlike conventional complexes of d-metals with electronegative ligands, compounds of the type under consideration are characterized by an inversion of the splitting of d-orbitals in the ligand field.**20** It is shown in Fig. 4 that the σ-donor orbitals of P atoms are higher in energy than the Fe 3d-orbitals. As a consequence, the e_g-bonding orbitals are predominantly metal orbitals utilized for the arrangement of the ligand electron pairs. Correspondingly, the ligand orbitals make a predominant contribution to $e_g{}^*$, the LUMO. The virtually nonbonding metal orbitals t_{2g} remain the HOMO. On passing from local levels to an extended structure, this implies that the position and the width of the band gap in the Zintl phase containing a d-metal depends, to a large extent, on the interaction energy between the d-metal and the main-group element.

The fulfillment of the octet rule by a main-group element is an important condition for the applicability of

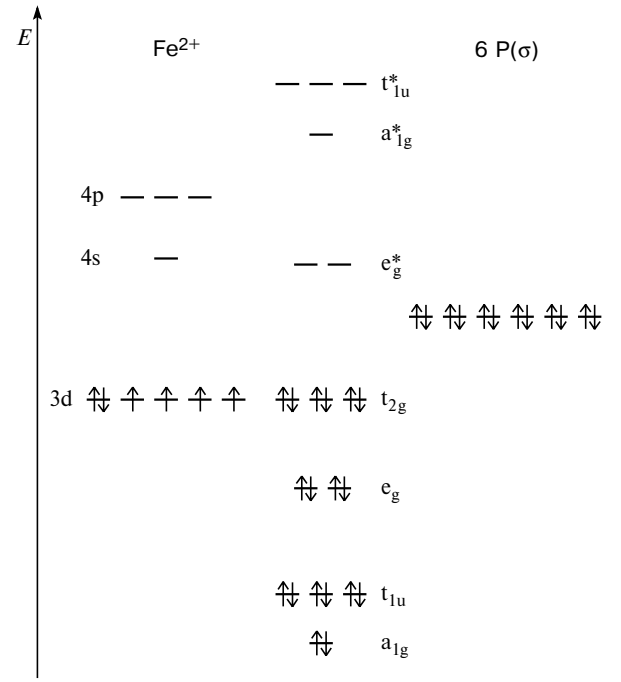

Fig. 4. MO diagram of the FeP_6 fragment; the octahedral coordination of Fe^{2+} ions corresponds to that observed in FeP_4; the dπ—pπ overlap is neglected.

the Zintl electron counting scheme to compounds with essentially covalent bonds. In the compound FeP_4 considered above, the $_\infty^2(P_4^{2-})$ layers are formed by two types of P atoms. Each of them has a tetrahedral environment, 2 P + 2 Fe or 3 P + 1 Fe. In the former case, the octet rule is fulfilled due to the formation of two homonuclear two-electron P—P bonds and the transfer of two electron pairs onto Fe orbitals. The electronic configuration of this P atom can be described as $3s^23p^4$, which corresponds to a −1 formal oxidation number. Similarly, the second independent P atom acquires the $3s^23p^3$ configuration corresponding to a zero formal oxidation state. In general, the number of homonuclear bonds formed by a main-group element, or connectivity (P), is strictly correlated with the formal oxidation state (Q). For Group 15 elements, this correlation is expressed by the equation $Q = P - 3$. Having returned to FeP_4, it can be easily seen that the formula of the $_\infty^2(P_4^{2-})$ polyanion reflects the presence of two- and three-bonded P atoms in 1 : 1 ratio.

When passing to Cd and Hg pnictidehalides, it should be borne in mind that the applicability of the above scheme to the description of the bonding is based on the assumption that the relatively electropositive Cd and Hg atoms form M^{2+} cations having the closed-shell d^{10} electronic configuration. Each pnicogen atom forms an electron octet due to the formation of homonuclear bonds and the transfer of electron pairs to Cd or Hg orbitals, while excess electrons are accepted by halogen atoms, which thus serve as X^- anions. Specific cases, for example, localization of the lone electron pair on the pnicogen atoms and the formation of Hg—Hg bonds, will be discussed where appropriate.

Classification of cadmium and mercury pnictidehalides

The classification of cadmium and mercury pnictidehalides $M_aZ_bX_c$ (M = Cd, Hg; Z = P, As, Sb; X = Cl, Br, I) is based on the type of the structural fragment formed by the Group 15 element (Table 1). Thus, series of compounds can be distinguished whose crystal structures contain (1) separate Z^{3-} anions; (2) binuclear Z_2^{4-} anions; (3) Z^{3-} anions and Z_2^{4-} bianions; (4) finite Z_3^{5-} anions; (5) one-dimensional infinite $_\infty^1(Z^-)$ polyanions.

The structure of the pnicogen fragment determines directly the connectivity and, correspondingly, the formal oxidation state of the pnicogen atom. These characteristics, in turn, are correlated with the stoichiometry

Table 1. Mercury and cadmium pnictidehalides $M_aZ_bX_c$ (M = Cd, Hg; Z = P, As, Sb; X = Cl, Br, I)

M	Z	Anion (connectivity of element Z) $a : b : c$						
		Z^{3-} (0)	Z^{3-}, Z_2^{4-} (0, 1)	Z_2^{4-} (1)			Z_3^{5-} (1, 2)	$_\infty^1(Z^-)$ (2)
		3 : 1 : 3; 5 : 2 : 4	4 : 2 : 3; 9 : 5 : 6	7 : 4 : 6	2 : 1 : 2	5 : 2 : 6; 8 : 7 : 1	7 : 6 : 4	2 : 3 : 1
Cd	P	Cd_3PCl_3,[21,22] Cd_3PI_3,[21] $Cd_5P_2Br_4$[26]	$Cd_4P_2Cl_3$,[23] $Cd_4P_2Br_3$,[25] $Cd_4P_2I_3$[27]	$Cd_7P_4Cl_6$[23]	—	—	—	Cd_2P_3Cl,[24] Cd_2P_3Br,[24] Cd_2P_3I[24]
	As	Cd_3AsCl_3,[24] Cd_3AsI_3[28]	$Cd_4As_2Cl_3$,[29] $Cd_4As_2Br_3$,[29] $Cd_4As_2I_3$[34]	—	Cd_2AsCl_2[30]	Cd_8As_7Cl[31]	—	Cd_2As_3Cl,[32] Cd_2As_3Br,[33] Cd_2As_3I[35]
	Sb	—	$Cd_4Sb_2I_3$[36]	—	Cd_2SbBr_2[37]	—	—	
Hg	P	Hg_3PCl_3,[38] $Hg_5P_2Br_4$[44]	$Hg_4P_2Cl_3$,[39] $Hg_9P_5I_6$[45]	$Hg_7P_4Br_6$[40]	Hg_2PCl_2[41]	—	$Hg_7P_6Br_4$[42]	Hg_2P_3Cl,[43] Hg_2P_3Br[43]
	As	—	$Hg_4As_2Br_3$,[46] $Hg_4As_2I_3$[48]	$Hg_{7.4}As_4Cl_6$[46]	Hg_2AsCl_2,[47] $Hg_{19}As_{10}Br_{18}$[47]	—	—	Hg_2As_3Br[33]
	Sb	—	$Hg_4Sb_2I_3$[36]	$Hg_7Sb_4Br_6$[49]	Hg_2SbBr_2[50]	$Hg_5Sb_2I_6$[51]	—	

and with the structure of compounds; therefore, phases containing the same anion formed by a Group 15 element often have identical compositions and similar structures.

Compounds containing only separate Z^{3-} anions either possess defect sphalerite or wurtzite structures,[21,22,28] or are analogs of the well-known salts of the Millon′s base.[26,44] The former type of structures has been studied rather comprehensively.[21] The description of the structure of Millon-base salts can be found in classical handbooks on inorganic crystal chemistry.[52]

In the series of cadmium and mercury pnictidehalides, compounds whose structure contains covalent bonds between the pnicogen atoms arouse the greatest interest. The change in the number and character of these bonds should have an influence on the properties of the phases in question. In this study, the attention is focused on pnictidehalides containing homonuclear bonds between Group 15 elements.

Compounds containing one-dimensional infinite $_{\infty}^{1}(Z^{-})$ anions

The family of pnictidehalides containing one-dimensional infinite $_{\infty}^{1}(Z^{-})$ anions is represented by compounds with the general formula M_2Z_3X (Table 2). The one-dimensional infinite $_{\infty}^{1}(Z)$ chains of Group 15 elements exist in all phases in the same conformation, which is unique and has never been encountered in the structures of binary pnictides. The helical polyanionic chains extend along the *c* axis of the unit cell (Fig. 5) and are linked by metal atoms. The three-dimensional framework thus formed has cavities in which halogen atoms are arranged.

The one-dimensional infinite polyanions of a pnicogen are composed of two crystallographically independent Z atoms in 2 : 1 ratio. Each atom has a more or less distorted tetrahedral environment consisting of two metal atoms and two pnicogen atoms (except for the Hg_2P_3Br structure [43]). The distances between the neighboring pnicogen atoms within a chain are typical of a single Z—Z covalent bond (Table 3). The cadmium—pnicogen distances are close to those in the structures of binary cadmium phosphides and arsenides, whereas binary mercury pnictides are unknown. Meanwhile, the distances from the halogen atoms to the metal atoms in all the Hg_2Z_3X structures are significantly greater than the length of a normal covalent bond in the corresponding binary crystal halides (see Table 3). There-

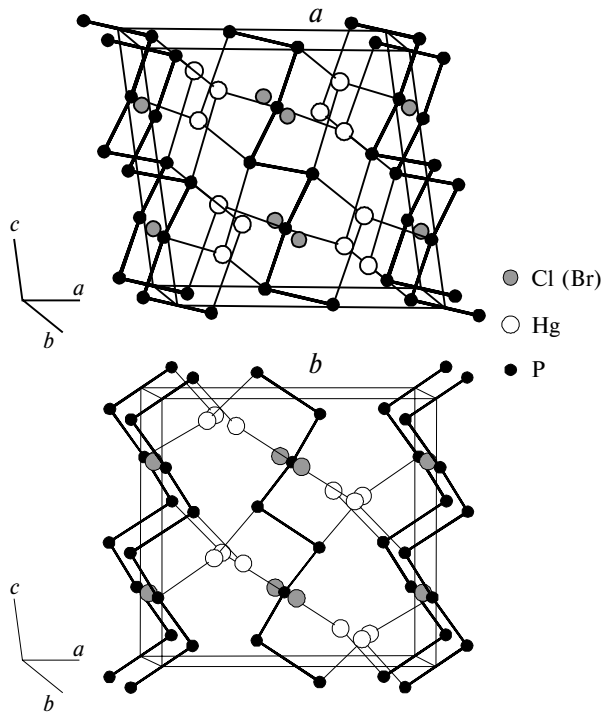

Fig. 5. Crystal structures of Hg_2P_3Cl (*a*) and Hg_2P_3Br (*b*); the bold lines show the P—P bonds in the $_{\infty}^{1}(P^{-})$ helical chains.

Table 2. Pnictidehalides M_2Z_3X (M = Cd, Hg; Z = P, As; X = Cl, Br, I)

Compound	Space group	Unit cell parameters				Ref.
		a	*b*	*c*	β /deg	
		Å				
Cd_2P_3Cl	*C*2/*c*	7.988(1)	8.988(1)	7.555(1)	100.91(5)	24
Cd_2P_3Br	*C*2/*c*	8.089(1)	9.089(1)	7.535(1)	100.36(5)	24
Cd_2P_3I	*C*2/*c*	8.255(1)	9.304(1)	7.514(1)	99.66(5)	24
Cd_2As_3Cl	*Cc*	8.265(1)	9.428(1)	7.974(1)	101.47(1)	32
Cd_2As_3Br	*C*2/*c*	8.281(1)	9.411(1)	7.993(1)	101.49(1)	33
Cd_2As_3I	*Cc*	8.436(1)	9.564(2)	7.952(2)	100.65(2)	35
Hg_2P_3Cl	*C*2/*c*	7.834(2)	8.844(1)	7.591(1)	98.68(1)	43
Hg_2P_3Br	*Pbcn*	8.014(1)	8.903(1)	7.823(1)		43
Hg_2As_3Br	*C*2/*c*	8.0914(8)	9.300(1)	8.1084(7)	99.32(1)	33

Table 3. Interatomic distances (*d*/Å) in M_2Z_3X (for comparison, the standard lengths (d_{cov}/Å) of the single bond between the corresponding atoms are given)

Compound	Z—Z		M—X		*d*(M—M)*
	d	d_{cov}	*d*	d_{cov}**[52]	
Cd_2As_3Br	2.42	2.52 [53]	2.82	2.79	3.780 (×1)
					3.904 (×1)
Cd_2As_3I	2.42—2.43	2.52 [53]	2.98—3.01	2.99	3.893 (×1)
					4.070 (×1)
Hg_2P_3Cl	2.19	2.22 [54]	2.99—3.04	2.23—2.27	3.363 (×1)
					3.916 (×1)
					4.261 (×1)
Hg_2P_3Br	2.20	2.22 [54]	3.17—3.34	2.45	4.112 (×1)
					4.192 (×2)
Hg_2As_3Br	2.43	2.52 [53]	3.10—3.24	2.45	3.461 (×1)
					4.134 (×1)

* The number of these bonds is given in parentheses.

** The metal—halogen distances in binary MX_2 halides are given.

fore, the structure of these phases can be described as a three-dimensional framework formed by the metal and pnicogen atoms with the halide anions located in the voids.

All the six possible phases have been found for cadmium,[24,32,33,35] while in the case of mercury, only three phases have been discovered, namely, Hg_2As_3Br,[33] Hg_2P_3Cl, and Hg_2P_3Br.[43] The specific features of Hg_2P_3Br deserve separate consideration. The structure of this phase differs substantially from the structures of other phases with this stoichiometry by the presence of chains with different chiralities in 1 : 1 ratio (see Fig. 5, *b*). This results in a changed coordination environment of Hg atoms; in the structure of Hg_2P_3Br, it consists of two closely located P atoms and three more distant Br atoms. The coordination of P atoms also changes. One of the two crystallographically independent P atoms resides (as in the structure of Hg_2P_3Cl) in the center of a tetrahedron formed by two other P atoms and two Hg atoms, whereas the second independent P atom is surrounded by two P atoms and one Hg atom, the fourth vertex of the tetrahedron being occupied by the lone electron pair (ψ-tetrahedral coordination in terms of the Gillespie model[55]). The number of P atoms with the ψ-tetrahedral coordination in the structure of Hg_2P_3Br is twice as great as the number of P atoms with the normal tetrahedral coordination. Unlike all the other compound of this family, which crystallize in the monoclinic system, Hg_2P_3Br belongs to the orthorhombic system. The above-described differences indicate that monoclinic distortion of its structure cannot result in the Hg_2P_3Cl (Hg_2As_3Br) structural type.

In accordance with the tetrahedral configuration of pnicogen (2 Z + 2 M), each pnicogen atom lends one electron for the formation of two homonuclear bonds and transfers one electron pair to the vacant orbitals of the two neighboring metal atoms, which corresponds to the $3s^23p^4$ and $3d^{10}4s^24p^4$ electronic configurations for P and As, respectively, and to their −1 formal oxidation numbers. In such a way the pnicogen atoms achieve their electron octets. In view of the oxidation numbers of the metal (+2) and the halogen (−1), it can be stated that the compounds under consideration are valence compounds, or Zintl phases that tend to exhibit semiconductor properties. This is consistent with the published data concerning determination of the type of conductivity of cadmium and mercury phosphide halides.[24,56] However, in the case of Hg_2As_3Br,[33] metallic conductivity has been found. Metallic properties of this compound are at variance with the predictions of the Zintl scheme because the formula $(M^{2+})_2(Z^-)_3(X^-)$ implies full occupancy of all the bonding levels, *i.e.* the formation of the filled valence band, while the conduction band remains empty.

The simplest model that accounts for the occurrence of metallic properties for Hg_2As_3Br is based on the overlap of the filled valence band with the empty conduction band, as shown in Fig. 6. Since conduction is

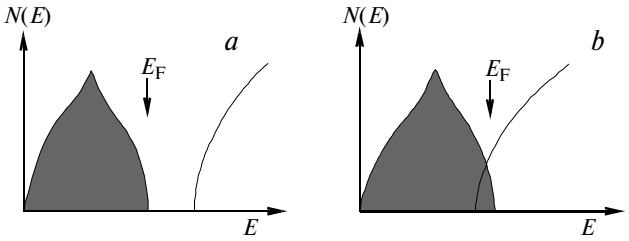

Fig. 6. Sketch of the band structures of Cd_2As_3Br and Hg_2P_3Br (*a*), and Hg_2As_3Br (*b*): the major contribution to the valence band (shaded) is made by the bonding M—Z and antibonding Z—Z interactions (*a*, *b*), and the conduction band is mainly formed from the antibonding M—X interactions (*a*), antibonding M—X and bonding M—M interactions (*b*). The approximate position of the Fermi level is marked (E_F).

not anisotropic,[33] the metal—pnicogen interactions are expected to make the major contribution either to the higher occupied levels or to the lower vacant levels. Then the change in the Hg—As interaction energy with respect to those of the Hg—P or Cd—As interaction should bring about the band overlap shown in Fig. 6. This purely qualitative model has found additional experimental evidence in a study of the metal—semiconductor concentration transition in the $Hg_2P_xAs_{3-x}Br$ solid solutions performed by electrical conductivity measurements and relaxation ^{31}P NMR spectroscopy.[57,58]

As noted above, the crystal structures of Hg_2As_3Br and Hg_2P_3Br are characterized by different types of chain chirality (the same configuration over the whole structure in the former case and alternation in 1 : 1 ratio in the latter case); therefore, these phases are not expected to form infinite solid solutions. Nevertheless, rather extended regions of homogeneity based on each phase were detected experimentally (Fig. 7);[58] this can be explained by the close similarity of the unit cell parameters of these phases (see Table 2). Electrical conductivity measurements for the monoclinic solid solution $Hg_2P_xAs_{3-x}Br$ have revealed metallic conductivity only for samples with $x \le 0.3$, while in the $0.3 < x < 0.6$ range of compositions, the metal—semiconductor concentration transition takes place as a result of statisti-

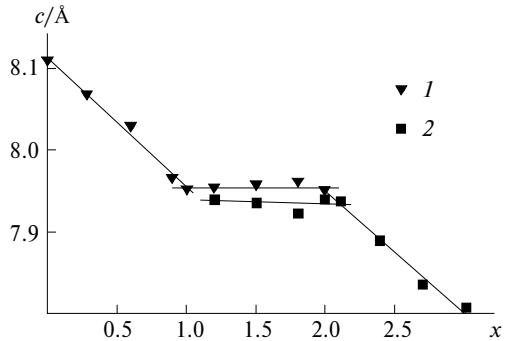

Fig. 7. Dependence of the unit cell parameter *c* on the composition of the $Hg_2As_{3-x}P_xBr$ solid solutions: monoclinic (*1*); orthorhombic (*2*).

cal[58,59] substitution of P atoms for the As atoms in the unidimensional infinite $_{\infty}^{1}(Z^{-})$ chains.

According to NMR spectroscopy data, the semiconductor—metal transition is accompanied by an abrupt change in the relaxation time (T_1) from 9.5 to 1.1 s, *i.e.*, almost by an order of magnitude.[57] The step in the $T_1(x)$ curve indicates that in the vicinity of the transition, the relaxation rate, *i.e.*, the intensity of interaction of the nuclear spin system with the lattice, markedly increases as a result of the appearance of an additional relaxation mechanism. This additional mechanism may be due to the fluctuating component of the magnetic field created by the conduction electrons at the point of the location of atoms. However, if the concentration of the conduction electrons is low, the increase in the relaxation rate (correspondingly, the decrease in the relaxation time) would be insignificant. This is confirmed by the experimental fact that the minimum T_1 value, equal to 1.1 s, is too great for "perfect" metals (*cf.* values of 0.1—0.01 s) and is normal for "poor" metals[60] with a vanishing band gap.

The conclusion that the Hg_2As_3Br and $Hg_2P_xAs_{3-x}Br$ ($0 < x \leq 0.3$) phases can be classified as "poor" metals was further confirmed by the band structure calculations performed on M_2Z_3X [61] using the extended Hückel method.[62] It can be seen from Fig. 8 that the major contribution to the valence band near the Fermi level is made in all cases by the metal—pnicogen bonding interactions and the pnicogen—pnicogen antibonding interactions. Substantial differences are observed in the bottom of the conduction band. Only in the case of monoclinic mercury-containing phases, do mercury—mercury bonding interactions make a substantial contribution to this region of the band structure. This specific feature of the band structures of these compounds is related to their crystal structure. Table 3 lists the shortest metal—metal contacts in the crystal structures of the four compounds under interest; it can be seen that relatively short mercury—mercury distances, 3.36 and 3.46 Å, respectively, are found only in Hg_2P_3Cl and Hg_2As_3Br. This difference between the metal—metal distances is consistent with the fact that mercury—mercury bonding interactions at the bottom of the conduction band are found only in the band structures of Hg_2P_3Cl and Hg_2As_3Br.

Further discussion of the band structures is hampered by the fact that extended Hückel calculations markedly overestimate the energy of the forbidden gap (E_g). It can only be suggested that in the case of Hg_2As_3Br, unlike Hg_2P_3Cl, the valence band overlaps with the conduction band, giving rise to the metallic type of conductivity. Evidently, the Hg—As binding interactions, responsible for the band overlap, are higher in energy than the corresponding Hg—P interactions. Thus, upon the replacement of As by P, or an increase in the content of phosphorus in $Hg_2P_xAs_{3-x}Br$, the levels that correspond to mercury—pnicogen binding interactions decrease in energy, and at $x = 0.3$, the energy gap (forbidden band) opens, thus bringing the system to the semiconductor state.

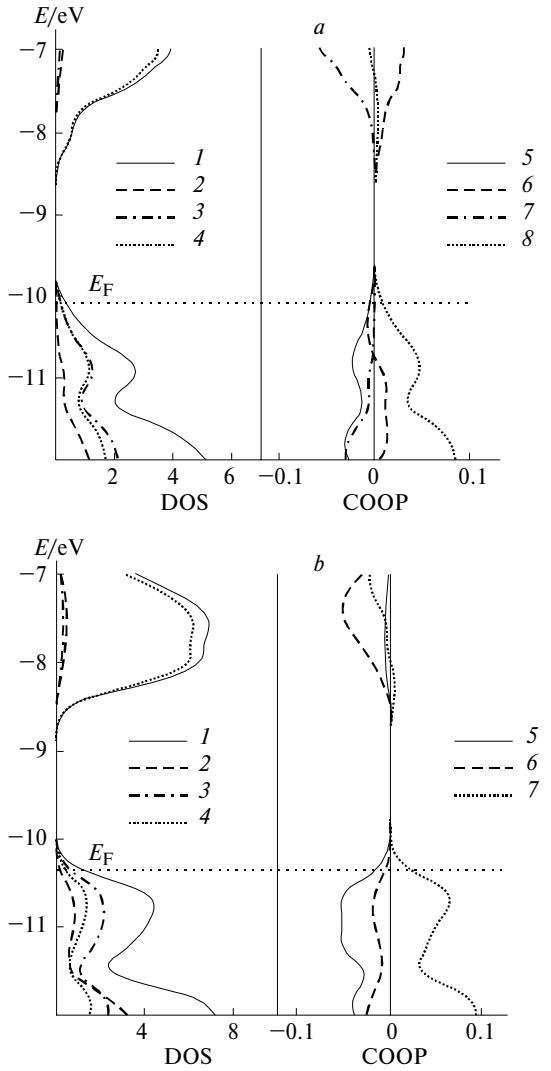

Fig. 8. Diagrams of the density of states (DOS) and the crystal orbital overlap population (COOP) for Hg_2P_3Cl (*a*) and Hg_2P_3Br (*b*) near the Fermi level (E_F). *a*. DOS: total (*1*), Cl (*2*), P (*3*), and Hg (*4*); COOP: P—P (*5*), Hg—Hg (*6*), Hg—Cl (*7*), and Hg—P (*8*). *b*. DOS: total (*1*), Br (*2*), P (*3*), Hg (*4*); COOP: P—P (*5*), Hg—Br (*6*), and Hg—P (*7*).

The Z_3^{5-} anions — breaking the chain

In the series of pnictidehalides, there is only one known example whose structure contains finite chain fragments formed by a Group 15 element. This is $Hg_7P_6Br_4$ and the solid solutions $Hg_7P_{6-x}As_xBr_4$ ($x \leq 2.3$).[42] The bent Z_3^{5-} anions are joined into a three-dimensional framework through Hg atoms. The coordination of the pnicogen atoms fully conforms to the Zintl—Klemm formalism, namely, two terminal Z atoms have three metal atoms as additional neighbors, whereas the central Z atom is coordinated to two Hg atoms

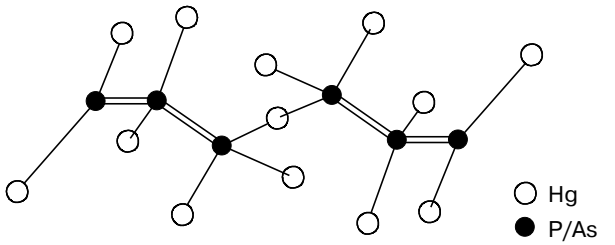

Fig. 9. The $[P_2As]^{5-}$ anion and its surrounding by Hg atoms in the crystal structure of $Hg_7P_{3.7}As_{2.3}Br_4$.

(Fig. 9). Thus, each pnicogen atom completes a distorted tetrahedral environment.

Compounds containing binuclear Z_2^{4-} anions

Almost in all cadmium and mercury pnictidehalides, the atom of a Group 15 element tends to acquire a tetrahedral environment to adopt an electron octet. As shown above, in the case of one-dimensional infinite polyanions, this results in each pnicogen atom forming two heteronuclear bonds with metal atoms, apart from the two homonuclear bonds. When the chain breaks giving rise to finite anionic fragments, the two terminal atoms acquire a different environment consisting of one homonuclear and three heteronuclear bonds. Removal of all the internal atoms results in the extreme case, namely, a fragment of two pnicogen atoms, each of them being bonded to three metal atoms and to one pnicogen atom. The Z_2^{4-} bianion is thus coordinated by six metal atoms.

In all the known cadmium and mercury pnictidehalides, the coordination number of the Z_2^{4-} anion, equal to 6, (Table 4) is realized as the Z_2M_6 octahedron (Fig. 10). The electronic structure of this polyhedron has been studied[41] in relation to the $(P_2Cd_6)^{8+}$ and $(P_2Hg_6)^{8+}$ model ions. It was found that the energy of every occupied MO of the P_2^{4-} ion decreases upon the interaction with the metal atom orbitals (Fig. 11). The P—Hg bond contains a substantial contribution of the mercury d-orbitals. The energy of the corresponding orbitals of Cd is too low; they cannot contribute significantly to the MO of the octahedron. This leads to an unusual phenomenon, namely, the P—Cd distances are longer than the P—Hg distances in similar compounds. The same feature has been found for octahedra with other pnicogens; however, on passing from phosphorus to antimony, this trend becomes less pronounced.

Analysis of the electronic structure provides the answer to yet another question: why is the environment of the Z_2^{4-} anion by metal atoms always octahedral? On the one hand (see Fig. 11), the atomic orbitals of phosphorus responsible for the formation of π- and π*-orbitals of the P_2^{4-} ion overlap with the Hg orbitals to give P—Hg σ-bonds. The loss of the π-component of the P—P bond should remove the obstacle to the rotation of one PHg_3 fragment relative to the other fragment around a three-fold axis. On the other hand, rotation through 60° would transform the octahedral coordination into a trigonal prism in which the distances between the Hg atoms of different PHg_3 fragments would become sufficiently short (~3.5 Å) for weak electrostatic Hg—Hg repulsion to arise.[61] Indeed, correlation calculations have demonstrated[41] that the octahedral configuration is ~0.2 eV energetically more favorable.

Table 4. Pnictidehalides containing binuclear Z_2^{4-} anions

Compound	Space group	Unit cell parameters				Ref.
		a	*b*	*c*	β /deg	
		Å				
$Cd_7P_4Cl_6$	*Pa*3	11.936				23
$Hg_7P_4Br_6$	$P2_1/c$	6.045	19.848	7.560	104.2	40
$Hg_{7.4}As_4Cl_6$	*Pa*3	12.178				46
$Hg_7Sb_4Br_6$	*Pa*3	12.994				49
$Cd_4P_2Cl_3$	*Pa*3	12.135				23
$Cd_4P_2Br_3$	*Pa*3	12.365				25
$Cd_4P_2I_3$	*Pbca*	12.890	12.725	12.654		27
$Cd_4As_2Cl_3$*	*Pa*3**	12.39				29
$Cd_4As_2Br_3$	*Pa*3**	12.64				29
$Cd_4As_2I_3$	*Pa*3	12.993				34
$Cd_4Sb_2I_3$	*Pa*3	13.488				36
$Hg_4P_2Cl_3$	*Pa*3**	11.828				39
$Hg_4As_2Br_3$	*Pa*3	12.610				46
$Hg_4As_2I_3$	*Pa*3	12.999				48
$Hg_4Sb_2I_3$	*Pa*3	13.439				36
$Hg_9P_5I_6$	$P2_1/c$	13.112	12.486	17.031	119.9	45
Cd_2AsCl_2	$P2_1/c$	7.858	9.193	8.189	119.95	30
Cd_2SbBr_2	$P2_1$	8.244	9.920	8.492	116.80	37
Hg_2PCl_2	$I2/m$	7.643	7.977	8.539	115.23	41
Hg_2AsCl_2	$C2/m$	13.914	8.210	8.896	97.61	47
$Hg_{19}As_{10}Br_{18}$	$P\bar{1}$	11.255	11.348	12.295	105.72***	47
Hg_2SbBr_2	$P2_1/c$	8.899	9.911	13.995	92.92	50
$Hg_5Sb_2I_6$	$Pc2_1n$	8.108	10.702	21.295		51
Cd_8As_7Cl	*Pa*3	7.266				31

* The composition of the compound is questionable.
** No structural data are available, the parameters were derived from powder X-ray diffraction data.
*** $\alpha = 105.73°$, $\gamma = 109.15°$.

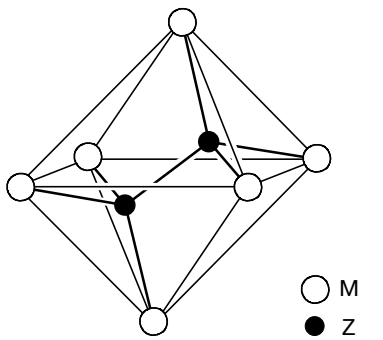

Fig. 10. View of the Z_2M_6 octahedron (Z = P, As, Sb; M = Cd, Hg).

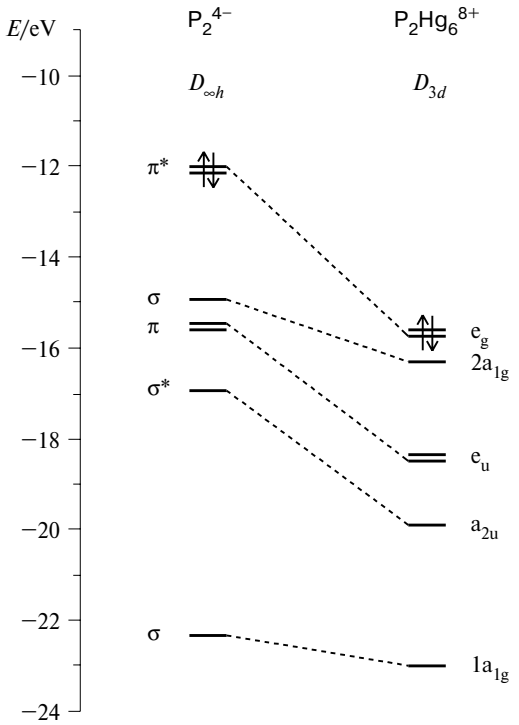

Fig. 11. MO diagram of the model octahedral ion $(P_2Hg_6)^{8+}$. The cation geometry corresponds to that shown in Fig. 10. The change in the energy of molecular orbitals of the P_2^{4-} fragment upon the interaction with six Hg atoms is shown. The vacant antibonding orbitals located high in energy are omitted for clarity.

Due to the high charge of the octahedron, the $[Z_2M_6]$ fragments in the majority of structures share vertices to give either a three-dimensional framework or two-dimensional layers. In the phases that contain separate Z^{3-} anions, in addition to binuclear Z_2^{4-} fragments, the octahedra are linked *via* ZM_4 tetrahedra.

The halogen atoms complete the coordination environment of the metal atoms, although the M—X distances are often much longer than the lengths of the corresponding covalent bonds found in binary crystalline halides. The substantial role of the halogen in ensuring the stability of the structures is additionally supported by the fact that binary mercury phosphides, arsenides, or antimonides are unknown, despite the great number of pnictidehalides formed by this metal.

Compounds $M_{7+\delta}Z_4X_6$

In the crystal structures of compounds with the general formula $M_{7+\delta}Z_4X_6$ (Fig. 12), the Z_2M_6 octahedra share all vertices to form a three-dimensional framework $[M_{6/2}Z_2] = [M_6Z_4]$. This gives a distorted "perovskite-like" sequence of octahedra containing two types of cavities; the larger cavities are occupied by MX_6 octahedra, while the smaller cavities accommodate separate metal atoms. However, not in all the structures of

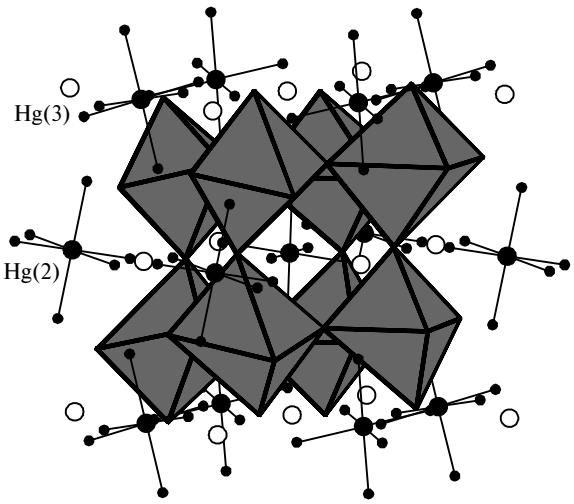

Fig. 12. Crystal structure of $Hg_{7.4}As_4Cl_6$; the framework constructed from the $[As_2Hg_6]$ octahedra sharing all vertices, the $HgCl_6^{4-}$ anions, and the Hg atoms filling the framework cavities are shown. The Hg(1) atom is an octahedron vertex.

the given series, does filling of the smaller cavities take place.

The most interesting feature of the cubic $Hg_{7+\delta}Z_4X_6$ phases[40,49] is the presence in the structure of metal atoms having a zero formal oxidation state. The Hg atoms can occupy three crystallographically independent positions, which differ substantially in coordination environment (Table 5). The M(1) position corresponds to atoms incorporated in the perovskite-like framework. This position is fully populated in the structures of all cubic phases. The M(1) atoms are linked to two pnicogen atoms. In addition, their coordination environment is supplemented by halogen atoms but the M(1)—X distances are markedly longer than typical covalent bonds (see Table 5). The M(2) and M(3) positions are located outside the framework; the former corresponds to metal atoms residing at the center of the octahedron formed by halogen atoms, while the latter corresponds to isolated metal atoms. If the M(2)—X distances are close to the lengths of the covalent bonds in binary crystalline halides, the coordination sphere of M(3) atoms (Fig. 13) is unusual and is never encountered in typical covalent compounds. The coordination sphere of these atoms consists of two pnicogen atoms, six halogen atoms, and six metal atoms. The so high coordination number (14) is rather typical of intermetallic compounds. In addition, the distances to the closest neighbors are so great (see Table 5) that interaction of the M(3) atoms with their neighbors can hardly be described as covalent bonds. Apparently, the M(3) atoms occur in a relatively low (close to zero) oxidation state. This suggestion is indirectly supported by the results of a solid-state ^{199}Hg NMR study[63] of $Hg_{7.4}As_4Cl_6$.

One should note a substantial difference between mercury compounds and the only cadmium compound belonging to this series. In $Cd_7P_4Cl_6$, unlike any

Table 5. Coordination environment of M(3) atoms and interatomic distances (d/Å) in $M_7Z_4X_6$

Compound	The distance from M(3) to the nearest neighbors			Metal—halogen distances		
				$M_7Z_4X_6$		MX_2,[52] d(M—X)*
	d(M(3)—X) (×6)*	d(M(3)—Z) (×2)*	d(M(3)—M(1)) (×6)*	d_{min}(M(1)—X)	d(M(2)—X) (×6)*	
$Cd_7P_4Cl_6$	—	—	—	2.76	2.66	2.66 (×6)
$Hg_{7.4}As_4Cl_6$	3.56	3.61	3.69	2.97	2.67	2.23 (×1), 2.27 (×1)
$Hg_{7.1}Sb_3AsBr_6$	3.83	3.33	3.53	3.29	2.80	2.45 (×2)
$Hg_7Sb_4Br_6$	3.92	3.32	3.57	3.33	2.81	2.45 (×2)

* The number of these bonds is given in parentheses.

$Hg_{7+\delta}Z_4X_6$ cubic phase, one Cl atom is located at a relatively short distance from the framework M(1) metal atom and no Cd atoms in the M(3) positions are present.

Proceeding from the structure and taking into account the fact that the average formal oxidation state of the pnicogen atoms in $M_{7+\delta}Z_4X_6$ is equal to −2, the crystal-chemical formula of these phases can be written as $[(M_6Z_4^{4+})(MX_6^{4-})M^0{}_\delta]$. The presence of zerovalent Hg atoms implies a deviation from the Zintl scheme because Hg^0 has neither an electron octet nor a stable d-configuration. However, the presence of formally zerovalent Hg atoms should not influence the electronic structure of compounds because low-energy orbitals of these atoms cannot affect significantly the structure of the top of the valence band. Generally, the expected dielectric properties peculiar to Zintl phases should be retained, which is supported by the appearance of these compounds, for example, $Hg_{7.4}As_4Cl_6$ forms light-brown crystals.

All the $M_{7+\delta}Z_4X_6$ pnictidehalides belong to the cubic space group *Pa*3 (see Table 4), except for the mercury phosphide bromide $Hg_7P_4Br_6$.[48] Its structure differs substantially from the structure of other compounds of this series described above. The three-dimensional framework formed by P_2Hg_6 octahedra is retained; however, neither $(HgBr_6)^{4-}$ octahedral anions nor separate metal atoms are located in the space between them. In addition, rotation of the octahedra around a pseudo-fourfold axis transforms the framework in such a way that each octahedron acquires one nonshared vertex (Fig. 14). The Br atoms complete the coordination of mercury. The formation of a cubic structure in this case is apparently precluded by the fact that the $(HgBr_6)^{4-}$ anions are too large and cannot fit into relatively small cavities of the $[Hg_6P_4]^{4+}$ framework (see below).

The compounds $M_4Z_2X_3$

This is the vastest class of pnictidehalides containing a Z_2^{4-} fragment. All compounds with this stoichiometry (see Table 4) are semiconductors and crystallize in the cubic system, except for $Cd_4P_2I_3$, which is orthorhombically distorted.[27] The structures of the $M_4Z_2X_3$ phases contain, in addition to the binuclear Z_2^{4-} anions, separate Z^{3-} anions whose coordination polyhedron is a tetrahedron formed by four metal atoms. The ZM_4 tetrahedra and the Z_2M_6 octahedra constitute a three-dimensional framework whose cavities are occupied by halogen atoms. The polyhedra are linked *via* common vertices; only polyhedra of different types are connected to one another. Since all the vertices of the Z_2M_6 octahedra are involved in the framework formation and the number of tetrahedra is twice as great as the number

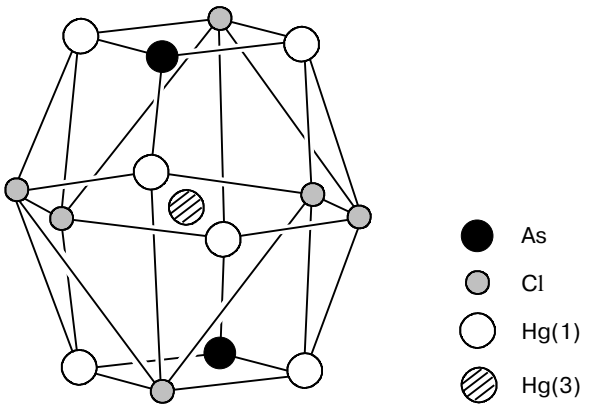

Fig. 13. Coordination environment of formally zerovalent Hg(3) atoms in the structure of $Hg_{7.4}As_4Cl_6$.

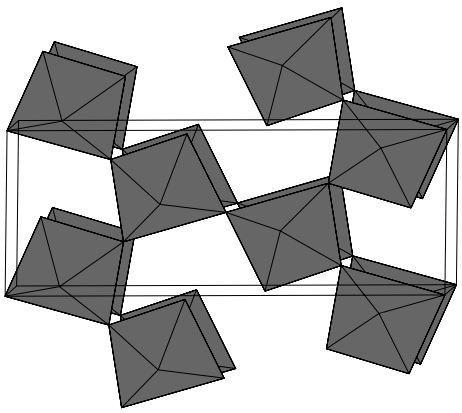

Fig. 14. Linkage of the P_2Hg_6 octahedra in the crystal structure of $Hg_7P_4Br_6$; the Br atoms are not shown.

of the octahedra, each tetrahedron has one nonshared vertex. The crystal-chemical formula of $M_4Z_2X_3$ can be written as $[(M^{2+})_8(Z^{3-})_2(Z_2^{4-})(X^-)_6]$.

It should be noted that the pnictidehalides $M_4Z_2X_3$ (4 : 2 : 3) and $M_{7+\delta}Z_4X_6$ (7 : 4 : 6) are structurally similar. Both compounds crystallize in the cubic space group *Pa*3 (except for the $Cd_4P_2I_3$ and $Hg_7P_4Br_6$, which have already been mentioned) with a unit cell parameter close to 12 Å. A study of the structures of ternary and substituted "*Pa*3-phases" [46] has resulted in a simple geometric scheme based on the ratio of the radii of the pnicogen and halogen atoms present in the structure (Fig. 15); the scheme illustrates the relationship between compounds with stoiciometric ratios of atoms equal to 4 : 2 : 3 and 7 : 4 : 6. It was shown (Table 6) that, when the r_Z/r_X ratio is greater than 1.11, the 7 : 4 : 6 structural type is stable, while for lower values, the stable type is 4 : 2 : 3. When $r_Z/r_X = 1.11$, phases of both structural types exist. As the ratio of the radii decreases to 0.83, an orthorhombic distortion of the 4 : 2 : 3 structure is observed. When $r_Z/r_X > 1.24$, the *Pa*3-phases are not formed.

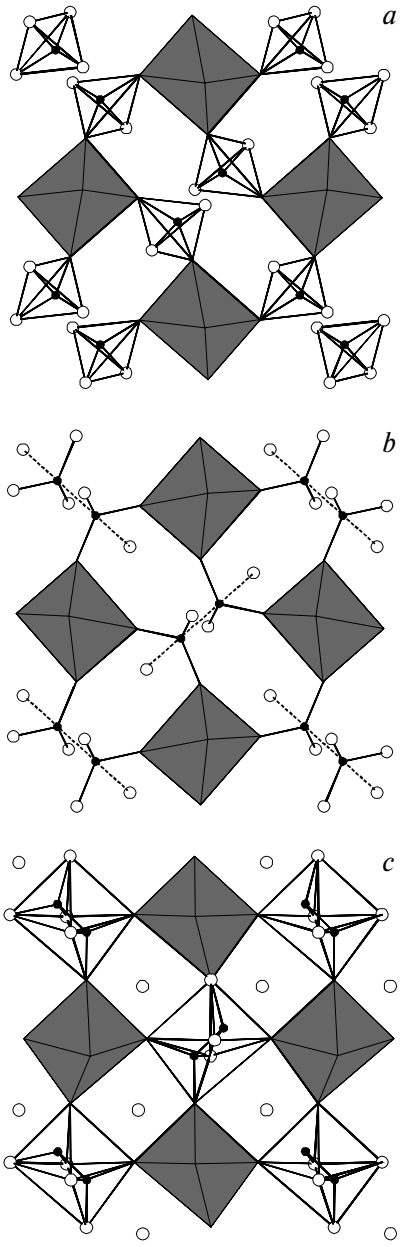

Fig. 15. Structural transformation 4 : 2 : 3 → 7 : 4 : 6 following a decrease in the halogen radius: crystal structure of $Hg_4As_2Br_3$ (*a*); intermediate (hypothetical) state (*b*); crystal structure of $Hg_{7.4}As_4Cl_6$ (*c*).

Table 6. Compositions of the *Pa*3 phases for different ratios of the radii of the Z and X atoms

Pairs of atoms Z/X	r_Z/r_X	Compounds
Sb/Cl	1.42	No *Pa*3 phases
Sb/Br	1.24	$Hg_7Sb_4Br_6$
As/Cl	1.22	$Hg_{7.4}As_4Cl_6$
P/Cl	1.11	$Cd_7P_4Cl_6$, $Cd_4P_2Cl_3$, $Hg_4P_2Cl_3$
As/Br	1.06	$Hg_4As_2Br_3$, $Cd_4As_2Br_3$
Sb/I	1.06	$Hg_4Sb_2I_3$, $Cd_4Sb_2I_3$
P/Br	0.96	$Cd_4P_2Br_3$
As/I	0.91	$Hg_4As_2I_3$, $Cd_4As_2I_3$
P/I	0.83	$Cd_4P_2I_3$,* $Hg_9P_5I_6$**

* Orthorhombic distortion, space group *Pbca*.
** Not a *Pa*3 phase but contains analogous structural fragments (see the text).

The $Hg_9P_5I_6$ phase with short Hg—Hg and P—P distances

In all the compounds described above, the Hg and Cd atoms occur in the oxidation state +2, except for the "guest" atom in the $M_{7+\delta}Z_4X_6$ type structure. The coordination of Cd and Hg atoms mainly complies with the view on the optimum arrangement of ligands around the central atom. In those cases where cadmium or mercury coordinate pnicogen and halogen atoms having relatively small size, octahedral coordination arises, for example, coordination of the M(2) atoms in $M_{7+\delta}Z_4X_6$. As the pnicogen and halogen radii increase, a coordination number equal to four becomes preferential. In both octahedral and tetrahedral coordinations, the Cd^{2+} and Hg^{2+} atoms have a closed-shell electron configuration, d^{10}; the contribution of the Hg d-orbitals to the chemical bond is relatively insignificant, while that for Cd atoms is negligibly small. However, in some cases, linear coordination of Hg atoms takes place. A significant contribution to the mercury—pnicogen bond is

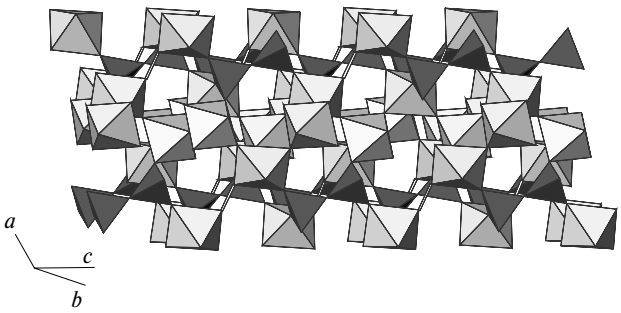

Fig. 16. Polyhedral representation of the crystal structure of $Hg_9P_5I_6$; the Hg—Hg bonds are outlined.

made[41] by the Hg d_{z2}-orbital, which is clearly manifested for $Hg_9P_5I_6$, possessing a unique structure.

A systematic study[64] has shown that this phase is the only ternary compound formed in the Hg—P—I system. The structure of $Hg_9P_5I_6$ [45] (Fig. 16) is an intricate framework composed of distorted P_2Hg_6 octahedra and P_2Hg_7 ditetrahedral groups, instead the separate ZM_4 tetrahedra present in $M_4Z_2X_3$. The octahedra share vertices thus forming layers parallel to the [100] plane. Four of the six Hg atoms in each octahedron are shared with other octahedra. The remaining free vertices are used to combine the octahedra into a three-dimensional framework through the P_2Hg_7 groups. The coordination environment of the Hg atoms belonging to only one octahedron is completed by the I atoms. These changes in the pattern of combination of the polyhedra (twinned tetrahedra instead of separate tetrahedra and links between the octahedra) result in a change in the P^{3-} to P_2^{4-} ratio from 2 : 1 in the $M_4Z_2X_3$ phases to 1 : 2 in $Hg_9P_5I_6$. As a consequence, the average formal oxidation state of the pnicogen atoms increases from −2.5 to −2.2 at the cost of the increase in the number of homonuclear bonds per Group 15 element atom.

The compound $Hg_9P_5I_6$ is the only known mercury phosphide iodide and the only compound with this stoichiometry among cadmium and mercury pnictide-halides. Moreover, its structure has two features unique for this type of compound. First, one of the ten crystallographically independent Hg atoms forms a homonuclear Hg—Hg bond (2.54 Å) and, formally, this atom is monovalent, whereas the other nine atoms are divalent. Thus, the crystal chemical formula of this substance can be written as $[Hg_2^{2+}(Hg^{2+})_{16}(P_2^{4-})_4(P^{3-})_2(I^-)_{12}]$. Second, the P—P distance in the binuclear anion (2.10 and 2.16 Å) is considerably shortened relative to the length of the single P—P bond (2.20 Å)[54] found in other phosphide halides and in most of binary phosphides. Simultaneously, the Hg—P distance increases, on average, by 0.15 Å. This indicates that the order of the P—P bond tends to increase due to the transfer of electrons from the P atoms (from the antibonding MO of the P_2^{4-} fragment) onto Hg atoms and that the Hg atoms tend to pass into the +1 oxidation state, which is fulfilled upon the formation of Hg—Hg bonds only for one of the ten crystallographically independent Hg atoms in the $Hg_9P_5I_6$ structure. The large energy difference between the 4d and 5s levels of the Cd atom precludes a linear coordination of cadmium and, hence, the formation of this type of compound.

The compounds M_2ZCl_2 and $Hg_{19}As_{10}Br_{18}$ with two-dimensional layers of the Z_2M_6 octahedra

The Z_2M_6 fragments combined with one another only upon sharing the equatorial vertices form two-dimensional infinite layers, $_\infty^2(Z_2M_4^{2+})$, which constitute the basis of structures of the M_2ZCl_2 series (see Table 4).

In the Hg_2PCl_2 and Hg_2AsCl_2 structures (Fig. 17),[41,47] the pattern of alternation of these layers along the *a* axis of the unit cell is analogous to that in K_2NiF_4.[52] Each equatorial Hg atom forms two bonds with pnicogen atoms, whereas for an axial Hg atom, only one bond of this type exists. The halogen atoms are located between the layer of octahedra thus completing the coordination environment of the Hg atoms. It can be seen from Table 7 that for the equatorial Hg atoms that ensure the combination of the octahedra into a layer, all Hg—Cl distances are relatively long compared to the covalent bond length in $HgCl_2$. However, the distance from each axial Hg atom to one Cl atom can be regarded as corresponding to a rather strong covalent bond. The direction of this bond is approximately normal to the $_\infty^2(Z_2M_4^{2+})$ layer. The other four Cl atoms are farther removed from mercury, each coordinating two metal atoms at an angle close to 180°; these Cl atoms together with the metal atoms are located in a plane nearly parallel to the layer of octahedra. Thus, the

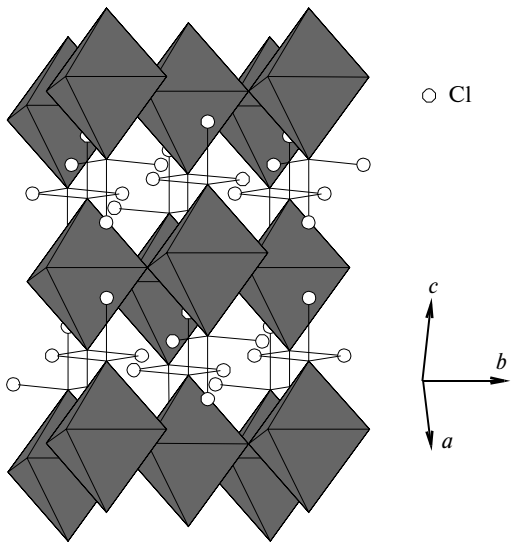

Fig. 17. Crystal structure of Hg_2AsCl_2; the alternation of layers formed by the $[As_2Hg_6]$ octahedra according to the K_2NiF_4 structural motif is shown.

Table 7. Most important distances (*d*) between the metal and halogen atoms in the structures of compounds of the M_2ZX_2 series and binary crystalline MX_2 halides

Compound	*d*/Å			
	M_2ZX_2			MX_2
	I*	II**	III***	
Cd_2AsCl_2	2.83—2.99	2.47	2.64—2.92	2.66
Cd_2SbBr_2	2.79—2.98	2.61	2.71—2.84	2.79
Hg_2PCl_2	3.23	2.39	2.82—3.15	2.23—2.27
Hg_2AsCl_2	3.09—3.22	2.38—2.42	2.70—3.49	2.23—2.27
$Hg_{19}As_{10}Br_{18}$	3.12—3.49	2.47—2.63	2.82—3.46	2.45

* For the equatorial vertices of the octahedron.
** For the axial vertices of the octahedron when the M—Z bond occupies the *trans*-position.
*** For the axial vertices of the octahedron when the M—Z bond occupies the *cis*-position.

coordination environment of the axial Hg atoms is a distorted octahedron.

In the case of cadmium, unlike mercury, the tetrahedral environment is more characteristic, which shows itself in the structures of most pnictidehalides. Therefore, although the structure of Cd_2AsCl_2 and Cd_2SbBr_2 is similar to the above-described structure of Hg_2PCl_2 and Hg_2AsCl_2, more stringent coordination requirements of Cd atoms bring about some distinctions. The Z_2Cd_6 octahedra within each layer are rotated in such a way (Fig. 18, *b*) that the Cd atoms located at their vertices acquire a distorted tetrahedral environment. Moreover, the layers of octahedra are not planar, as in the case of the corresponding mercury compounds but are somewhat distorted. Thus, the structure is modified being "adjusted" to the corresponding metal. As in the case of mercury-containing phases, the equatorial Cd atoms form two bonds with the pnicogen atom and, hence, their coordination environment is supplemented by two halogen atoms. The axial Cd atoms form one Cd—Z bond and three Cd—X bonds.

The structure of $Hg_{19}As_{10}Br_{18}$ is a superstructure of Hg_2AsCl_2 in which 2/5 of all the octahedra are characterized by the ordered absence of the Hg atom at one vertex, which is replaced by a lone electron pair (see Fig. 18, *c*).[47] Thus, the coordination environment of some As atoms is a trigonal pyramid formed by one pnicogen atom and two metal atoms rather than a distorted tetrahedron formed by one pnicogen atom and three metal atoms. The distance from the Hg atoms to the halogen atoms that complete its coordination sphere vary over a very broad range (see Table 7). A feature peculiar to Hg_2PCl_2 and Hg_2AsCl_2 is retained, namely, whereas the Hg—Br distances for the equatorial Hg atoms are much longer than the covalent bond length in crystalline $HgBr_2$, for each axial Hg atom, one of the distances is close to the Hg—Br bond length in mercury dibromide.

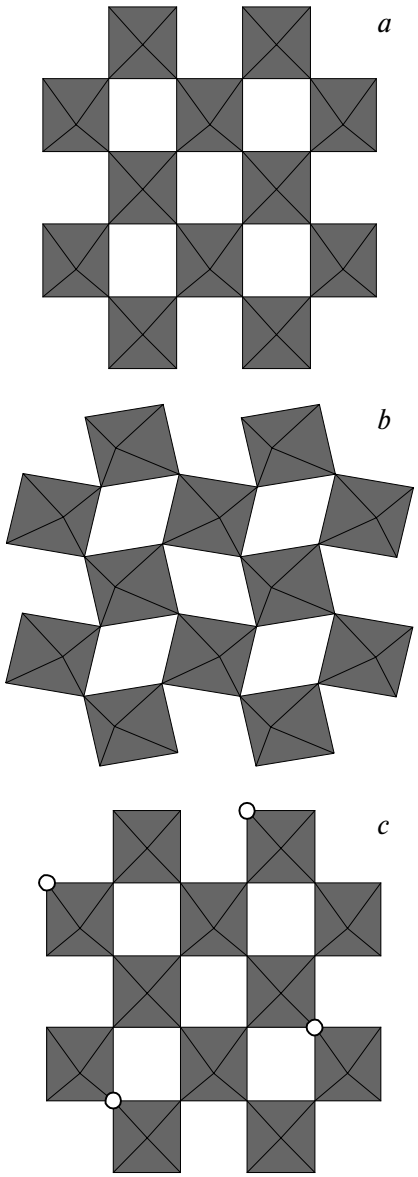

Fig. 18. Top view of the layers of octahedra in the structures of Hg_2AsCl_2 (*a*), Cd_2AsCl_2 (*b*), and $Hg_{19}As_{10}Br_{18}$ (*c*); the circles mark the positions of vacancies at the vertices of the octahedra.

The $Hg_5Sb_2I_6$ phase

The structure of $Hg_5Sb_2I_6$ [51] contains binuclear Sb_2^{4-} anions surrounded by five metal atoms. This fragment can be represented as an octahedron in which one vertex is missing, $Z_2M_5\square$. Thus, the structure contains Sb atoms of two types. One Sb atom is located at the center of the tetrahedron formed by three Hg atoms and one Sb atom. The environment of the other Sb atom consists of two Hg atoms and one Sb atom, which are located at vertices of a distorted tetrahedron whose fourth vertex is occupied by the lone electron pair (ψ-tetrahedral coordination of Sb). The Sb—Sb distance (2.82 Å) is some-

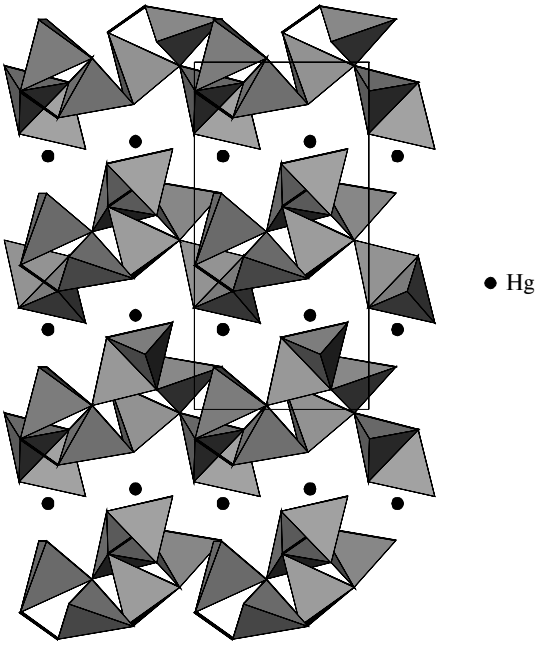

Fig. 19. Projection of the crystal structure of $Hg_5Sb_2I_6$ onto the [100] plane. The layers formed by the $HgSbI_3$ tetrahedra are shown; the black circles correspond to the Hg atoms combining the layers into a three-dimensional framework; the bold lines show the Sb—Sb bonds.

what longer than that in $Hg_7Sb_4Br_6$ (2.77 Å) or in $Hg_4Sb_2I_3$ (2.75 Å), which is quite understandable because one vertex of the Sb_2M_6 octahedron in $Hg_5Sb_2I_6$ is vacant.

The SbI_3 tetrahedron with a Hg atom located at the center can be considered as an alternative approach to the description of the crystal structure of $Hg_5Sb_2I_6$ (Fig. 19). In this case, this compound can be regarded as being related in structure to mercury iodide. The orange modification of HgI_2 is formed[52] by corrugated layers consisting of HgI_4 tetrahedra sharing vertices and edges. In the $Hg_5Sb_2I_6$ structure, these layers are composed of $HgSbI_3$ tetrahedra and are less symmetric due to the presence of short Sb—Sb distances between the corresponding tetrahedron vertices. In addition, the layers are connected to one another by bridging Hg atoms.

The Cd_8As_7Cl phase as a specific case

The crystal structure of Cd_8As_7Cl (Fig. 20), like those of many other cadmium and mercury pnictidehalides, contains the As_2^{4-} bianions. Nevertheless, it differs essentially from other phases because each of the As atoms contained in the bianion forms, apart from the As—As bond, four As—Cd bonds, and, hence, its coordination number is five.[31] The environment of the As_2^{4-} fragment is a distorted cube formed by Cd atoms in which the As_2^{4-} anion is arranged along a fourfold axis. This unusual coordination of As atoms is seldom encountered, for example, it is found in cadmium arsenide

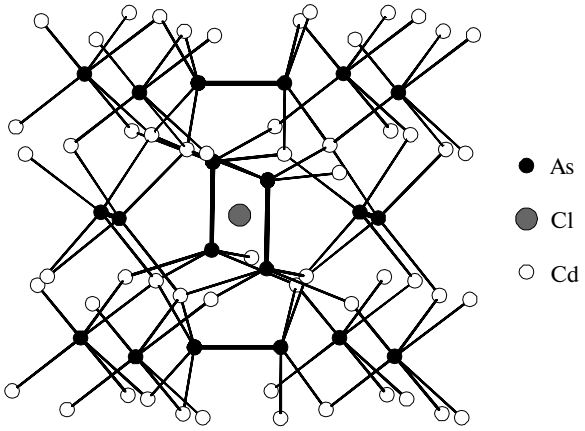

Fig. 20. Crystal structure of Cd_8As_7Cl.

(CdAs) prepared at high pressure.[65] This structure also contains As atoms coordinated by four Cd atoms forming a tetrahedron.

The Cd atoms are statistically distributed over two close positions with partial occupancies to form a slightly distorted tetrahedral environment consisting of either four As atoms or three As atoms and one Cl atom. Apparently, the distribution of cadmium over two positions results in a more favorable coordination of the As and Cl atoms and, what appears to be more important, allows the Cd atoms to realize a tetrahedral environment peculiar to them (d^{10} configuration).

Analysis of the MO diagram for the main structural fragment $(Cd_8As_2)^{12+}$ (point group D_{4h}) reveals two important features of the electronic structure (Fig. 21). First, the s-orbitals of the As atoms (σ_s- and σ_s*-MO of

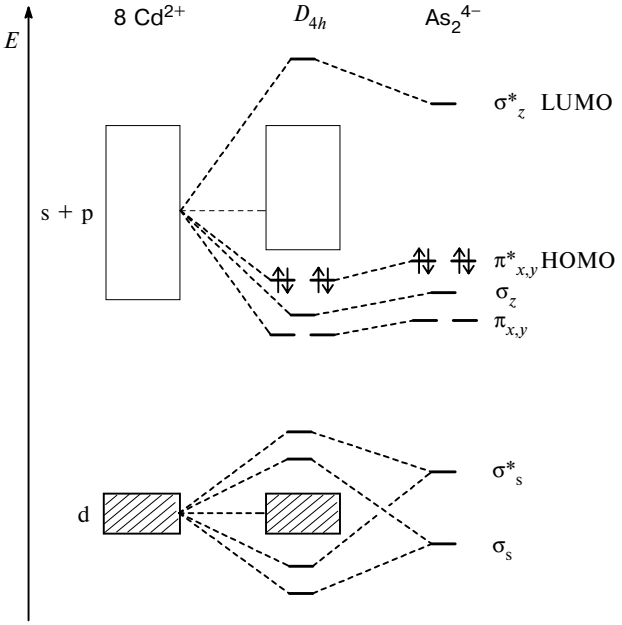

Fig. 21. Elementary diagram of the molecular orbitals of the model $(Cd_8As_2)^{12+}$ ion.

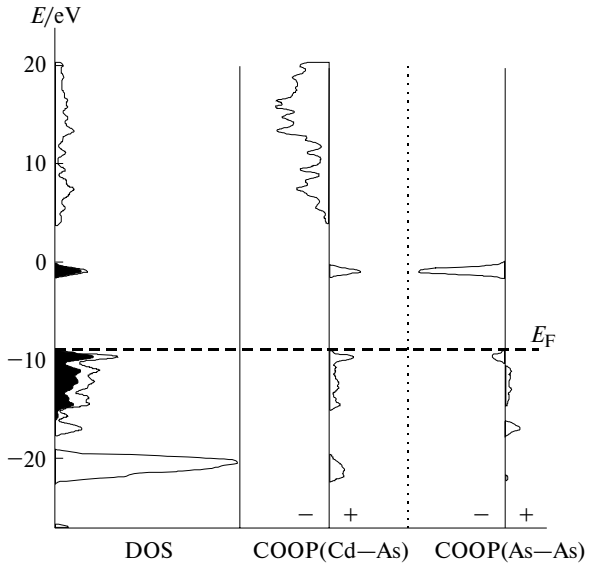

Fig. 22. Band structure of Cd_8As_7Cl: total DOS and partial DOS for the As_2^{4-} fragments (colored black); the COOP is given for the Cd—As and As—As bonds (E_F is the Fermi level).

As_2^{4-}) interact with the cadmium d-orbitals; however, these orbitals lie low in energy and the resultant MO do not make a substantial contribution to the electronic structure of Cd_8As_7Cl. Second, the p-orbitals of the As atoms (σ_z-, $\pi_{x,y}$-, and $\pi_{x,y}$*-MO of As_2^{4-}) interact only with the s- and p-orbitals of Cd atoms giving rise to three sets of low-lying occupied orbitals. Vacant, mainly nonboding orbitals of the Cd atom are located above them in energy. The orbital located next in energy is the vacant MO formed mainly by the only vacant antibonding σ_z* orbital of the As_2^{4-} bianion. However, the band structure calculation of Cd_8As_7Cl showed that it is these orbitals (altogether, three of them in a unit cell) that form a narrow acceptor band which is the lowest unoccupied crystal orbital (Fig. 22). This is attributable to the fact that, in the formation of a three-dimensional structure, the s- and p-orbitals of the Cd atoms, which are nonbonding orbitals for the $(Cd_8As_2)^{12+}$ fragment, interact with orbitals of the As^{3-} and Cl^- anions to give occupied bonding and vacant antibonding crystal orbitals. It is the alternation of different anions in the primitive cubic packing of Cd atoms that might be responsible for the stabilization of Cd_8As_7Cl.

* * *

The cadmium and mercury pnictidehalides surveyed in this review are the Zintl phases, more precisely, nontraditional Zintl phases. In recent years, the number of so-called nontraditional or boundary Zintl phases has steadily increased. More and more publications devoted to alkali and alkaline earth metal aluminides and Zintl phases containing transition metals now appear.[66] The more complicated the chemical composition of these compounds, the more pronounced the deviations from the classical Zintl scheme. First of all, this refers to the formal oxidation states of elements and the charge distribution. Specific features of chemical bonding often result in an unusual distribution of the electron density. For example, in $MoNiP_8$, in which the connectivity and the electron configuration formally correspond to each other, quantum-chemical calculations show the presence of a substantial negative charge on Ni atoms.[20] A similar situation, *i.e.*, a negative charge on Au atoms, has been discovered[67] in $K_4AuTlSn_3$. The discrepancy between the charge and the oxidation number by no means discards the Zintl approach to the description of valence compounds. Moreover, the octet rule, or, on a broader scale, the rule of "closed-shell electron configuration" makes it possible to identify the atomic orbitals used in the formation of chemical bonds in each compound considered. Thus, we can predict the properties of compounds and, moreover, propose the methods for modifying these properties by atomic substitutions aimed finally at the development of new and promising materials.[68] Then the extension of the initial concept of valence compounds becomes a tool that can be used to perform the primary analysis of any compound at the border of the Zintl phases.[69] There also exist additional approaches contributing to this task. Among them, note the concept of site preference energy,[70] which has been forgotten but is now widely used again; in combination with the Zintl—Klemm concept, this would enable predicting the pattern of ordered substitution in the complex Zintl phases and, hence, provide the possibility of more and more targeted design of compounds with specified composition, structure, and properties.

This work was supported by the Russian Foundation for Basic Research (Project No. 00-03-32539a) and the St. Petersburg Center of Fundamental Natural Sciences (Project No. 9-144).

References

1. R. Nesper, *Prog. Solid State Chem.*, 1990, **20**, 1.
2. J.-T. Zhao and J. D. Corbett, *Inorg. Chem.*, 1995, **34**, 378.
3. R. Ramirez, R. Nesper, H. G. von Schnering, and M. C. Bohm, *J. Phys. Chem. Solids*, 1987, **48**, 51.
4. C. Zheng and R. Hoffmann, *Z. Naturforsch., Teil B*, 1986, **41**, 292.
5. R. Hoffmann and C. Zheng, *J. Phys. Chem.*, 1985, **89**, 4175.
6. T. Y. Kuromoto, S. M. Kauzlarich, and D. J. Webb, *Chem. Mater.*, 1992, **4**, 435.
7. A. V. Shevelkov, E. V. Dikarev, R. V. Shpanchenko, and B. A. Popovkin, *J. Solid State Chem.*, 1995, **114**, 379.
8. R. Nesper, J. Curda, and H. G. von Schnering, *Angew. Chem., Int. Ed. Engl.*, 1986, **25**, 350.
9. B. Eisenmann and R. Kniep, *Z. Anorg. Allg. Chem.*, 1991, **589—590**, 213.
10. K. H. Lii and R. C. Haushalter, *J. Solid State Chem.*, 1992, **67**, 374.
11. J.-T. Zhao and J. D. Corbett, *Inorg. Chem.*, 1994, **33**, 5721.
12. E. Zintl and W. Dullenkopf, *Z. Phys. Chem.*, 1932, **B16**, 195.

13. P. C. Schmidt, D. Stahl, B. Eisenmann, R. Kniep, V. Egert, and J. Kubler, *J. Solid State Chem.*, 1992, **97**, 93.
14. M. Asbrand, F. J. Berry, B. Eisenmann, R. Kniep, L. E. Smart, and R. C. Thied, *J. Solid State Chem.*, 1995, **118**, 397.
15. R. B. King, *Inorg. Chem.*, 1989, **28**, 3048.
16. G. Menge and H. G. von Schnering, *Z. Anorg. Allg. Chem.*, 1976, **422**, 219.
17. W. Jeitschko and D. J. Braun, *Acta Crystallogr., Sect. B*, 1978, **34**, 3196.
18. D. J. Braun and W. Jeitschko, *Z. Anorg. Allg. Chem.*, 1978, **445**, 157.
19. H. Krebs, K. H. Müller, and G. Zürn, *Z. Anorg. Allg. Chem.*, 1956, **285**, 15.
20. M. Llunell, S. Alvarez, P. A. Alemany, and R. Hoffmann, *Inorg. Chem.*, 1996, **35**, 4683.
21. A. Rebbah, J. Yazbeck, and A. Deschanvres, *Rev. Chim. Miner.*, 1981, **19**, 43.
22. A. V. Shevelkov, E. V. Dikarev, and B. A. Popovkin, *Zh. Neorgan. Khim.*, 1997, **42**, 1242 [*Russ. J. Inorg. Chem.*, 1997, **42** (Engl. Transl.)].
23. A. V. Shevelkov, L. N. Reshetova, and B. A. Popovkin, *J. Solid State Chem.*, 1998, **137**, 138.
24. P. C. Donohue, *J. Solid State Chem.*, 1972, **5**, 71.
25. I. Kassama, M. Kheit, and A. Rebbah, *J. Solid State Chem.*, 1994, **113**, 248.
26. M. M. Shatruk, L. N. Reshetova, A. V. Shevelkov, and B. A. Popovkin, *Zh. Neorg. Khim.*, 2000, **45**, 565 [*Russ. J. Inorg. Chem.*, 2000, **45** (Engl. Transl.)].
27. A. Rebbah, J. Yazbeck, and A. Deschanvres, *Acta Crystallogr., Sect. B*, 1980, **36**, 1747.
28. A. Rebbah, J. Yazbeck, and A. Deschanvres, *Acta Crystallogr., Sect. B*, 1980, **36**, 1744.
29. L. Suchow and N. R. Stemple, *J. Electrochem. Soc.*, 1963, **110**, 766.
30. A. Rebbah, J. Yazbeck, A. Leclaire, and A. Deschanvres, *Acta Crystallogr., Sect. B*, 1980, **36**, 771.
31. A. V. Shevelkov, L. N. Reshetova, and B. A. Popovkin, *J. Solid State Chem.*, 1997, **134**, 282.
32. S. M. Gasinets, M. V. Potorii, I. D. Olekseyuk, E. A. Yantso, and M. I. Markovich, *Ukr. Khim. Zh.*, 1990, **56**, 123.
33. A. V. Shevelkov, E. V. Dikarev, and B. A. Popovkin, *J. Solid State Chem.*, 1994, **113**, 116.
34. J. Gallay, G. Allais, and A. Deschanvres, *Acta Crystallogr., Sect. B*, 1975, **31**, 2274.
35. A. Rebbah, A. Leclaire, J. Yazbeck, and A. Deschanvres, *Acta Crystallogr., Sect. B.*, 1979, **35**, 2197.
36. A. V. Shevelkov, E. V. Dikarev, and B. A. Popovkin, *J. Solid State Chem.*, 1991, **93**, 331.
37. L. N. Reshetova, A. V. Shevelkov, and B. A. Popovkin, *Zh. Koordinats. Khim.*, 1999, **25**, 819 [*Russ. J. Coord. Chem.*, 1999, **25** (Engl. Transl.)].
38. P. Lemoult, *C. R. Acad. Sci.*, 1907, **9**, 1175.
39. A. V. Olenev, Degree Thesis, Moscow State University, Moscow, 1998, 70 pp. (in Russian).
40. A. V. Shevelkov, E. V. Dikarev, and B. A. Popovkin, *J. Solid State Chem.*, 1996, **126**, 24.
41. A. V. Olenev, A. V. Shevelkov, and B. A. Popovkin, *J. Solid State Chem.*, 1998, **142**, 14.
42. A. V. Shevelkov, M. Yu. Mustyakimov, M. M. Shatruk, and B. A. Popovkin, *Zh. Neorgan. Khim.*, 1998, **43**, 1069 [*Russ. J. Inorg. Chem.*, 1998, **43** (Engl. Transl.)].
43. A. V. Shevelkov, E. V. Dikarev, and B. A. Popovkin, *Z. Kristallogr.*, 1994, **209**, 583.
44. A. V. Shevelkov, M. Yu. Mustyakimov, E. V. Dikarev, and B. A. Popovkin, *J. Chem. Soc., Dalton Trans.*, 1996, 147.
45. M. Ledésert, A. Rebbah, and Ph. Labbé, *Z. Kristallogr.*, 1990, **192**, 223.
46. A. V. Shevelkov, E. V. Dikarev, and B. A. Popovkin, *J. Solid State Chem.*, 1993, **104**, 77.
47. A. V. Shevelkov, E. V. Dikarev, and B. A. Popovkin, *Zh. Neorgan. Khim.*, 1995, **40**, 1496 [*Russ. J. Inorg. Chem.*, 1995, **40** (Engl. Transl.)].
48. Ph. Labbé, M. Ledésert, B. Raveau, and A. Rebbah, *Z. Kristallogr.*, 1989, **187**, 117.
49. A. V. Shevelkov, E. V. Dikarev, and B. A. Popovkin, *J. Solid State Chem.*, 1992, **98**, 133.
50. H. Puff and H. Gotta, *Z. Anorg. Allg. Chem.*, 1966, **343**, 225.
51. A. V. Shevelkov, E. V. Dikarev, and B. A. Popovkin, *Z. Anorg. Allg. Chem.*, 1994, **620**, 389.
52. A. F. Wells, *Structural Inorganic Chemistry*, 5th ed., Clarendon Press, Oxford, 1984.
53. H. G. von Schnering, *Angew. Chem., Int. Ed. Engl.*, 1981, **20**, 33.
54. H. G. von Schnering and W. Hönle, *Chem. Rev.*, 1988, **88**, 243.
55. R. J. Gillespie and I. Hargittai, *The VSEPR Model of Molecular Geometry*, Allyn and Bacon, Boston, 1991.
56. P. C. Donohue, *J. Solid State Chem.*, 1973, **6**, 587.
57. E. N. Morozova, Degree Thesis, Moscow State University, Moscow, 1997, 61 pp. (in Russian).
58. M. M. Shatruk, Ph. D. Thesis (Chem.), Moscow State University, Moscow, 2000, 164 pp. (in Russian).
59. M. M. Shatruk, A. V. Olenev, A. V. Shevelkov, and B. A. Popovkin, *Zh. Neorgan. Khim.*, 1997, **42**, 1610 [*Russ. J. Inorg. Chem.*, 1997, **42** (Engl. Transl.)].
60. J. Winter, *Magnetic Resonance in Metals*, Clarendon Press, Oxford, 1971, 297 pp.
61. L. A. Bengtsson-Kloo and A. V. Shevelkov, *Final Report on the SI Grant*, Lund University, 1998, 7 pp.
62. J. H. Ammeter, H. B. Bürgi, J. C. Thibeaut, and R. Hoffmann, *J. Am. Chem. Soc.*, 1978, **100**, 3686.
63. A. V. Shevelkov, *VI European Conf. Solid State Chem., Book of Abstracts* (*Zürich, September 17—20*), Zürich, 1997, ML7.
64. M. Yu. Mustyakimov, Degree Thesis, Moscow State University, Moscow, 1995, 70 pp. (in Russian).
65. J. Clark and K. J. Range, *Z. Naturforsch., Teil B*, 1976, **31**, 158.
66. *Chemistry, Structure and Bonding of Zintl Phases and Ions*, Ed. S. M. Kauzlarich, VCH Publishers, New York, 1996, 245.
67. D. Huang and J. D. Corbett, *Inorg. Chem.*, 1998, **37**, 5007.
68. M. M. Shatruk, K. A. Kovnir, and A. V. Shevelkov, VII *European Conf. Solid State Chem., Book of Abstracts (Madrid, September 15—18*), Madrid, 1999, O11.
69. M. M. Shatruk, K. A. Kovnir, A. V. Shevelkov, I. A. Presniakov, and B. A. Popovkin, *Inorg. Chem.*, 1999, **38**, 3455.
70. G. J. Miller, *Eur. J. Inorg. Chem*, 1998, 523.

Received November 21, 2000;
in revised form January 15, 2001